Numerical simulation of universal and Adiabatic Quantum Computation by Time Crystal: Proposal of Quantum Time Crystal Computing

Hikaru Wakaura[1] and Andriyan B. Suksmono[2]

1 : QuantScape Inc., 4-11-18, Manshon-Shimizudai, Meguro, Tokyo, 153-0064, Japan
2 : Institut Teknologi Bandung, Jl. Ganesha No.10, Bandung, Jawa Barat, Indonesia

Abstract. The time crystal is a well-known phenomenon observed in any quantum Floquet system. Time Crystal is a phenomenon in which the states of the system propagate spontaneously, saving time-reversal symmetry. It is one of many body localisations that prolong the lifetime of quantum states. However, it is destroyed by the operation from external environments such as gate operations. Therefore, we propose the method to Control the Time Crystal by modifying the Hamiltonian and driving noise conserving time-reversal symmetry. As a result, the method demonstrated the simple gate operations, Grover's, and Quantum Fourier Transformation algorithms by Time Crystal. We also demonstrated adiabatic Grover's and Shor's algorithm.

Keywords: Quantum computing, Quantum algorithm, Time Crystal.

1 Introduction

Chaotic phenomena have been studied for a century. Such phenomena are investigated and demonstrated in quantum physics, such as quantum chaos, quantum integrable systems, quantum non-integrable systems, and many-body localization. Integrable quantum many-body systems are characterized by an abundance of conserved quantities, which endow them with remarkable properties such as complete solvability and regular behavior. These systems exhibit a high degree of order and simplicity, allowing for exact analytical solutions and revealing deep connections to mathematical structures such as integrable models and algebraic techniques. Examples of integrable systems include the Heisenberg one-dimensional model [14], the Lieb-Liniger one-dimensional model [15], and the Tonks-Girardeau gas [24], among others. Conversely, non-integrable quantum many-body systems lack such conserved quantities and exhibit chaotic dynamics, leading to complex emergent behavior. The absence of integrability results in phenomena such as thermalization, where the system reaches a state of maximum entropy and loses memory of its initial conditions. Non-integrable systems are ubiquitous in nature and encompass a wide range of physical phenomena, including thermalization in quantum gases [23], quantum chaos in black holes [22], and the onset of turbulence in fluid dynamics [38].

In parallel, the concept of many-body localization [1] has emerged as a cornerstone in the study of quantum thermalization and ergodicity. Many-body localization refers to the phenomenon wherein quantum information remains localized within individual regions of a disordered quantum system, inhibiting the system's ability to thermalize and equilibrate. This departure from conventional statistical mechanics has profound implications for our understanding of quantum phase transitions and the stability of quantum coherence in interacting systems. Many-body localization has emerged as a cornerstone in the study of

David C. Wyld et al. (Eds): ADCO, CMCA, NeCoM, NLPI, CSITEC, BDBS, DMML, SP – 2025
pp. 147-166, 2025.CS & IT -CSCP 2025 DOI: 10.5121/csit.2025.150513

quantum thermalization and ergodicity. Many-body localization refers to the phenomenon wherein quantum information remains localized within individual regions of a disordered quantum system, inhibiting the system's ability to thermalize and equilibrate. This departure from conventional statistical mechanics has profound implications for our understanding of quantum phase transitions and the stability of quantum coherence in interacting systems. For these reasons, chaotic phenomena are utilized in computing applications, such as image encryption [32, 40]. Quantum chaos is also harnessed for computation in various ways. One prominent example is the Quantum Reservoir Computer, which leverages chaotic behavior that emerges through measurement and feedback mechanisms[6, 41, 19]. Other studies focus on circuits designed to induce quantum chaos [31], two-level chaotic systems [18], and the application of Shor's algorithm in quantum integrable systems [25].

Time crystals (TCs), first proposed by Nobel laureate Frank Wilczek in 2012 [39], represent a paradigm shift in our understanding of equilibrium dynamics. Unlike traditional notions of equilibrium, where temporal symmetry is preserved, TCs exhibit a spontaneous breaking of time translation symmetry, manifesting as persistent oscillations even in the absence of external driving. This unique feature offers tantalizing prospects for the exploration of new phases of matter with potential applications in quantum computing and precision metrology. In fact, some groups in the world have demonstrated that Discrete Time Crystal [8] [5] makes the lifetime of qubits longer.

In addition, the group at Aalto University announced that TCs could be used as qubits, and they have a long lifetime above 2 seconds after the crossing of energy levels [4]. Controlling of the quantum state by the TC phase itself may be realized unless time-reversal symmetry is preserved.

The gate operation destroys the time-reversal symmetry. However, the noise modification can propagate the quantum state to the aimed state, conserving the time-reversal symmetry. Therefore, we propose a novel method of quantum calculation that takes advantage of Time crystals. We call this Quantum Time Crystal Computing (QTCC). The optimal Hamiltonians and parameters vary depending on the aimed and initial states. The parameters can be optimized by the manner of Quantum Machine Learning (QML) [17][13]. QML is the hybrid method using a quantum computer and classical machine learning methods, such as Quantum Circuit Learning (QCL) and Quantum Support Vector Machine (QSVM) [27], Quantum Neural Network (QNN) [2] [20], and Born Machine (BM) [21]. We use the Hamiltonian Engineering Born Machine (HEBM) [36], which is the specialized BM for optimizing the parameters of Hamiltonians for aimed propagation. The HEBM is applicable for material engineering such as Variational Quantum Eigensolver and its family [33]. Hence, HEBM can optimize the parametric Hamiltonians and realize QTCC. It may broaden the scope of quantum computers and become the clue to finding a novel quantum system. We performed the flipping of all qubits, making an evenly distributed state, Grover's algorithm, Shor's algorithm and Quantum Fourier Transformation (QFT) by QTCC with optimized parametric Hamiltonians.

Section 1 is the introduction, section 2 describes the method detail of QTCC and the optimization method, section 3 describes the result for flipping and evenly distributed state, 4 shows the result of universal and adiabatic Grover's algorithm, the result of QFT, and the result of adiabatic Shor's algorithm, Section 5 is the discussion of results, and section 6 is the concluding remark.

2 Method

This section describes the details of Quantum Time Crystal Computing (QTCC) and our demonstration. Time Crystal (TC) is a symmetrical propagation of quantum systems

with time-reversal symmetry. It is demonstrated on several quantum Floquet systems, such as the ring of spin and photons. Hamiltonian varies periodically between radiated by an electromagnetic field and noisy system propagated by a Hamiltonian with randomized coefficients corresponding to the noise. Any quantum system can be in the TC phase, and the TC prolongs the lifetime of quantum systems as,

$$H = \begin{cases} \sum_{j=0}^{N} 0.5(1-d)X_j & (0 \leq t \ mod \ 2T \leq T) \\ H_1 & (T < t \ mod \ 2T \leq 2T). \end{cases} \tag{1}$$

N is the number of qubits and H_1 includes the noises and d is the assumed tunable coefficient, which is 0.001 for all calculations.

We assume the noise of this term as the rotation noise of parameters such as $\{\theta_i = \theta_i^0 + \theta_i^r Err(0, 1/3)\}$, Where $Err(0, 1/3)$ is the Gaussian function which the center is $x = 0$ and standard deviation is 1 /3. We use a Hamiltonian Engineering Born Machine (HEBM) to derive the desired parameters, which realize the aimed distribution of probabilities. Any superpositioned state can be realized by optimizing and modifying the parameters. The scheme of HEBM is almost the same as that of the Quantum Machine Learning (QML) algorithms [30]. It minimizes the Loss functions such as,

$$F = \boldsymbol{f} K \boldsymbol{f} + \boldsymbol{f^{aim}} K \boldsymbol{f^{aim}} - 2\boldsymbol{f^{aim}} K \boldsymbol{f}. \tag{2}$$

and or KL divergence

$$D_{KL}(\boldsymbol{f^{aim}} \| \boldsymbol{f}) = \sum_{i=0}^{N-1} \boldsymbol{f}_i^{\boldsymbol{aim}} \cdot \left(\log \boldsymbol{f}_i^{\boldsymbol{aim}} - \log \boldsymbol{f}_i \right) \tag{3}$$

where $\boldsymbol{f}$ is the calculated distribution of probability obtained by time propagation of the initial state by parametric Hamiltonians, and $\boldsymbol{f^{aim}}$ is their aimed value, respectively. This is the maximum-mean-discrepancy-loss (MMD-loss) function. Then, $\boldsymbol{f}$ and $\boldsymbol{f^{aim}}$ are calculated distributions that are derived by the parametric quantum circuit and aimed distribution, respectively.

They are 2^N-dimensional vectors and expressed as $\boldsymbol{f}_j = \mid x_j \mid^2$ for $U \mid \Phi_{ini} \rangle = \mid \Phi \rangle = \sum_{j=0}^{2^N-1} x_j \mid j \rangle$ and $\boldsymbol{f}_j^{\boldsymbol{aim}} = \mid f_j \mid^2$ for $\mid \Phi_{ans} \rangle = \sum_{j=0}^{2^N-1} f_j \mid j \rangle$ by the decimal state represented by the state of each qubit.

In addition, $\boldsymbol{f}$ can be substituted for the coefficients derived by quantum tomography. Quantum tomography [7] is a method for estimating quantum states from the trace of density matrices of states and Pauli operators. The states can be identified by the 4^N-dimensional vector.

$$\begin{aligned} \rho = \frac{1}{2^N} \sum_{\mu_1=0}^{3} \sum_{\mu_2=0}^{3} \cdots \sum_{\mu_N=0}^{3} Tr[(\sigma_{\mu_1} \otimes \sigma_{\mu_2} \otimes \cdots \otimes \sigma_{\mu_N})\rho] \\ \cdot \ \sigma_{\mu_1} \otimes \sigma_{\mu_2} \otimes \cdots \otimes \sigma_{\mu_N}. \end{aligned} \tag{4}$$

Then, 0, 1, 2, and 3 of Pauli matrices indicate that they are the I, X, Y, and Z operators for a given qubit, respectively. We use the Hamiltonian propagator and the propagator is expressed as $U = exp(-i/2Hdt)^{N_{dt}}$ for $\pi = 2dtN_{dt} = 2T$. The parameters are coefficients of Hamiltonians, and Hamiltonians are expressed in Pauli's words. Then N_{dt} is the number of time frames and is fixed at 50. Hamiltonian takes the form $H = \sum_{j=0}^{N_o-1} \theta_j P_j$ for the product of the Pauli matrix P_j, consisting of the Pauli matrix X_j, Y_j, Z_j. N_o is the number of P_j in Hamiltonian.

Hence, the propagator must be decomposed into propagators of single terms of Hamiltonian. It is achieved by Suzuki-Trotter decomposition [29] in this work. In this method, the Born machine is used for Hamiltonian engineering. This is why we call this method HEBM (Fig. 1).

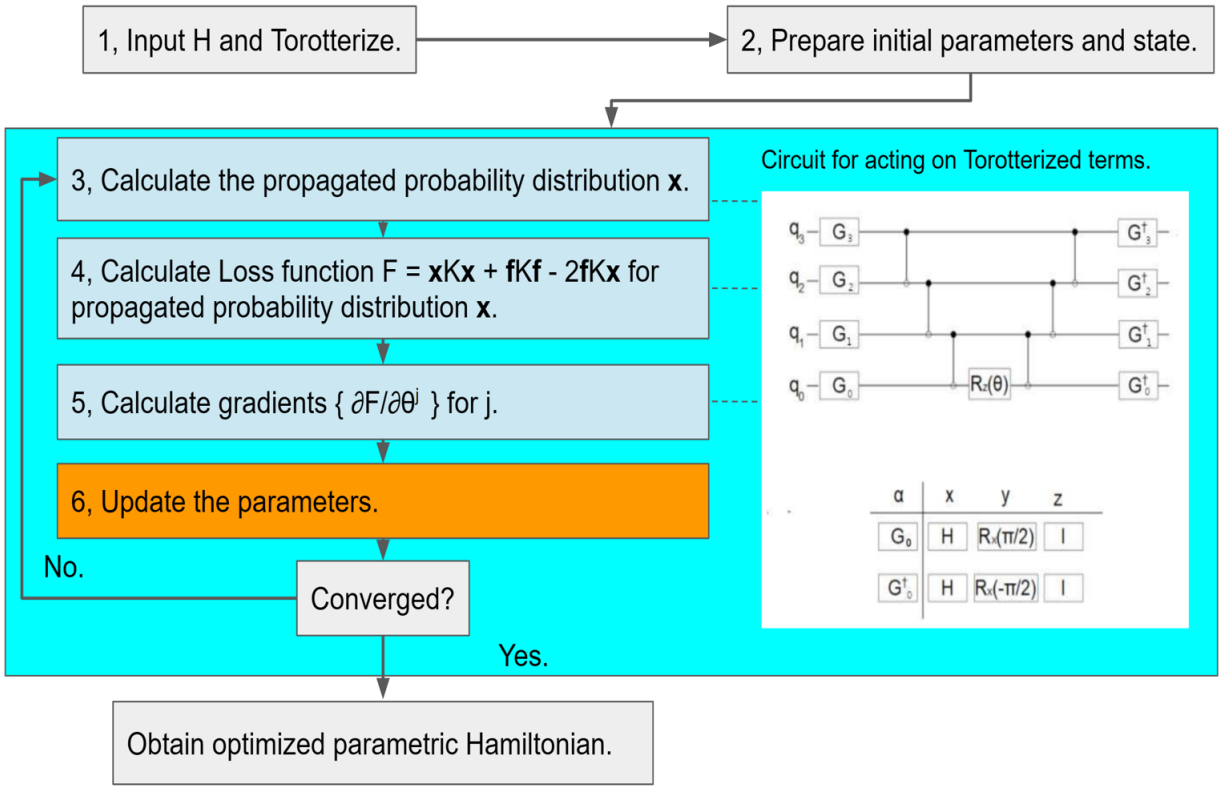

Fig. 1. The flowchart of HEBM[36]. 1, Firstly, parametric Hamiltonian H is input and Trotterized. 2, The initial parameters are set on H, and the initial circuit $\mid \Phi_{ini} \rangle$ is prepared. 3, The initial state is propagated by H using the circuit depicted by $t = \pi/2$. 4, The loss function F is calculated for the final calculated distribution $\mid \Phi \rangle = exp(-iHt/2) \mid \Phi_{ini} \rangle$. 5, The gradients of the loss function are calculated according to the parameter shift rule (PSR). 6, The parameters are updated by gradients. If the conditions of convergence are satisfied, final parameters and Hamiltonian are obtained. Otherwise, 3, 4, 5, and 6 are performed using updated parameters.

The method of optimizing variables is the Covariance Matrix Adaptation Evolutionary Method (CMaEs) [12] because optimization, including noisy parameters, cannot be performed accurately by Heuristic methods such as Broyeden-Fretcher-Goldfarb-Shanno (BFGS) and Nelder-Mead methods. CMaEs is an optimization method that searches for the optimum parameters by estimating the parameter sets in parameter space and weighting each parameter set.

By iterating this, the CMaEs method searches for the global minimum. The evaluation function is the average of eq. 2 or 3 for 10 results of propagation. We use blueqat

SDK [16] for numerical simulation of quantum calculations and optionally [3] to optimize parameters.

3 Discrete TC and time-reversal symmetry

In this section, we perform QTCC for flipping all qubits and making an evenly distributed state by optimizing parameters. In these simulations, $H_1 = \sum_{j=0}^{3}(\theta_j^{ZXZ} Z_{j-1} X_j Z_{1+1})$ for $j = -1 = 4 = 0$ the third term of parent Hamiltonian for Gibbs distribution of 1-D Ising model. The result of flipping all qubits is shown in Figs. 2 and 3. The Values of the evaluation function for the number of trials are shown in Fig. 2, and the probability of each state for the time frame by gradation map is shown in Fig. 3, respectively. We calculate the evaluation function at t = 2T.

The realm of the parameter is [0 ,2) for all value components from here without declare.

As shown in Fig. 2, the 800th trial lowers the evaluation function, and the minimum average of the evaluation function result in 10 sampling is nearly 4.1837 $\times 10^{-3}$ for the 755th trial. Fig. 3 shows the probability of each state for a time frame by gradation map. At that time, the 2T and 4T stare of qubits go back to the $|\,0\rangle$ state. However, the first qubit from the left is depolarized at 4T, and the second qubit is depolarized at 5T respectively. Even though time-reversal symmetry is almost preserved. This means the acceleration of DTC can be achieved by adjusting the amount of noise.

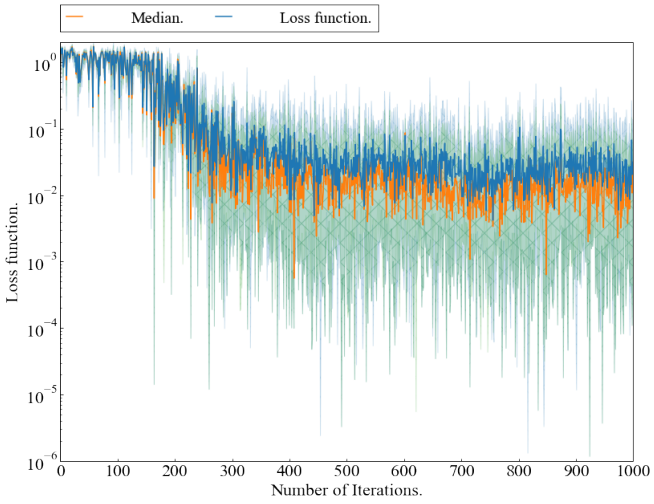

Fig. 2. The number of trials v.s. the average of the loss function for the $|\,0\rangle$ state in case the initial state is the $|\,0\rangle$ state, and the Hamiltonian is the third term of the parent Hamiltonian for Gibbs distribution of 1-D Ising model. The blue area is the realm of the distribution of loss function for 10 sampled values, and the green hatched area is the standard deviation, respectively.

The result of an evenly distributed state is shown in Figs. 4 and 5. The Values of the evaluation function for the number of trials are shown in Fig. 4, and the probability of each state for the time frame by gradation map is shown in Fig. 5, respectively. We calculate the evaluation function at t = 4T. Shown in Fig.4, the average of the evaluation function is lowered from the 700th trial, and the minimum is 1.8 $\times 10^{-2}$ at the 929th trial. The minimum of the result in 10 samplings is 8.0535 $\times 10^{-3}$, and the maximum is 4.0242 $\times 10^{-2}$, and the median is 1.3655 $\times 10^{-2}$, respectively.

Fig. 5 shows that the rebound of probability from the evenly distributed state at 6T and 8T even rebounded states are $|\,13\rangle$ and $|\,14\rangle$, respectively.

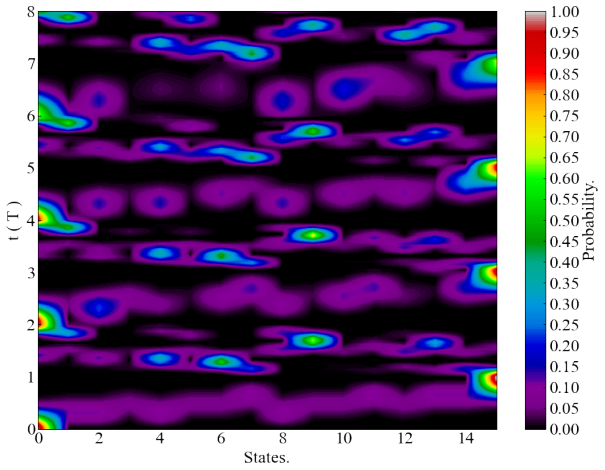

Fig. 3. The probability of states for time expressed by gradation map at 755 th trial for the $|\,0\rangle$ state in case the initial state is the $|\,0\rangle$ state and the Hamiltonian is the third term of the parent Hamiltonian for Gibbs distribution of 1-D Ising model.

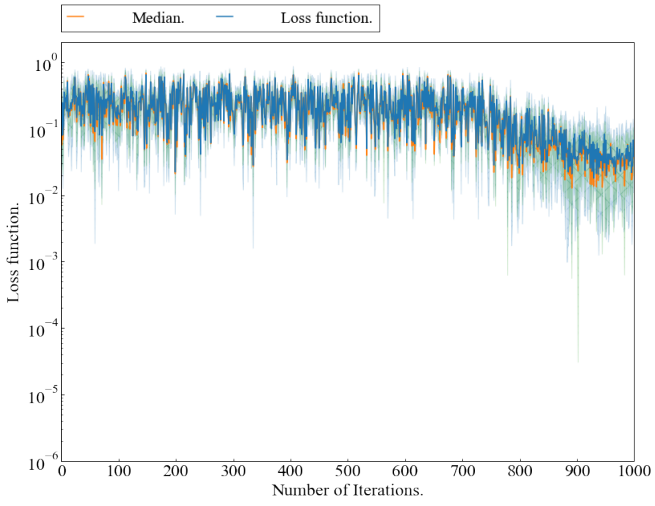

Fig. 4. The number of trials v.s. the average of the loss function for the evenly distributed state in case the initial state is the $|\,0\rangle$ state, and the Hamiltonian is the third term of the parent Hamiltonian for Gibbs distribution of 1-D Ising model. The blue area is the realm of the distribution of loss function for 10 sampled values, and the green hatched area is the standard deviation, respectively.

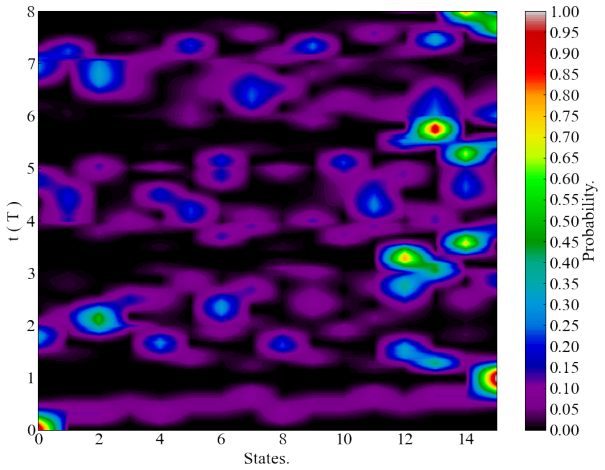

Fig. 5. The probability of states for time expressed by gradation map at 929th trial for the evenly distributed state in case the initial state is the $|0\rangle$ state and the Hamiltonian is the third term of the parent Hamiltonian for Gibbs distribution of 1-D Ising model.

The DTC started from an evenly distributed state and never propagated to a given one state in only 8T by positive parameters, with noise below 2 with respect to broadness. QTCC may have a chaotic mechanical system if the Hamiltonian parameters are positive or negative.

4 Grover's and Quantum Fourier algorithm on QTCC

In this section, we perform Grover's algorithm and Quantum Fourier Transformation (QFT) [35] on QTCC and show the results. We calculated the evaluation function at t = 2T for all cases in this section. The Hamiltonians for time propagation are the third term of the Gibbs distribution, the All—to—All connected Ising model, and the One-body Pauli X and Z operators, respectively. We added the oracle operator for the following section for all Hamiltonians, Hence, the third term of Gibbs distribution, All—to—All connected Ising model, and One-body Pauli X and Z operators have 10, 22, and 18 parameters, respectively. Aimed data is $|0\rangle$ state for all following calculations

4.1 Grover's algorithm on universal and adiabatic quantum computers

In this section, we demonstrate Grover's algorithm and discuss the result using QTCC in a universal and adiabatic manner. We calculate the evaluation function at t = 2T. At first, we derive the parametric set for the three above types of Hamiltonians for quarter Grover's operator on the 3-qubit system. Figs. 6, 8, and 10 indicate the logarithmic loss functions for the third term of Gibbs distribution, All-to-All connected Ising, and One-body Pauli X and Z, respectively. As shown in Fig. 6, Gibbs distribution is the most accurate in three Hamiltonians and kept lowering at 1500 th trial.

In Contrast, All-to-All Ising has the lowest accuracy of three, as shown in Fig. 8. The convergence is the firstest. The One-body Pauli X and Z have both middle accuracy and a time for convergence. as shown in Fig. 10. In Figs. 7, 9, and 11, we show the probability distributions for time on three types of Hamiltonians. All cases are far from Grover's operator's goal regarding the distribution. The distribution peak may not be feasible with only positive or negative parameters because the chaotic motions are fundamentally irreversible.

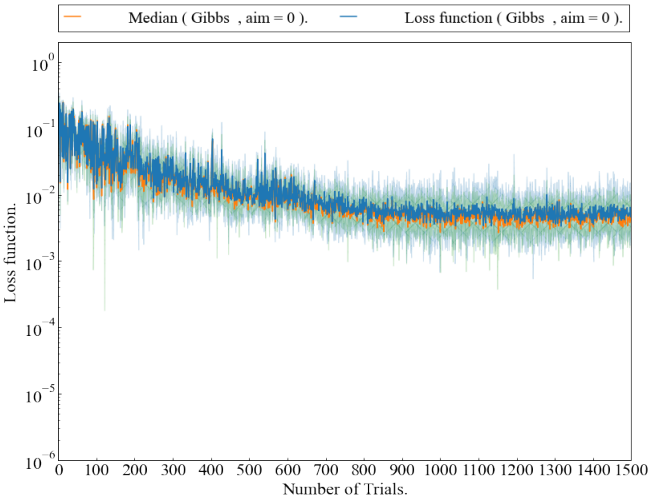

Fig. 6. The number of trials v.s. the average of the loss function for the quarter Grover's operator in case the initial state is the evenly distributed state, and the Hamiltonian is the third term of the parent Hamiltonian for Gibbs distribution of 1-D Ising model. The blue area is the realm of the distribution of loss function for 10 sampled values, and the green hatched area is the standard deviation, respectively.

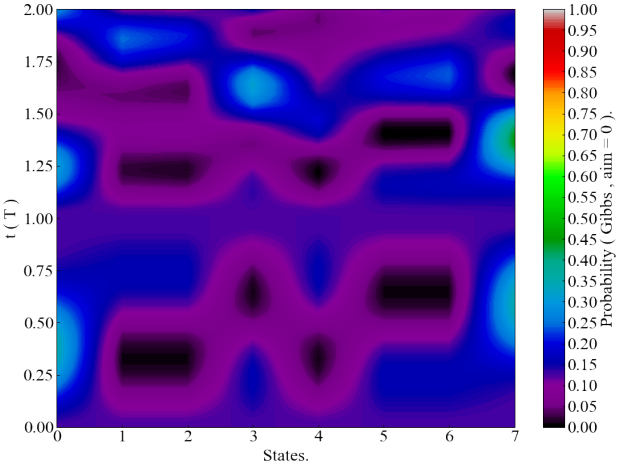

Fig. 7. The probability of states for time expressed by gradation map at the best trial for the quarter Grover's operator in case the initial state is the evenly distributed state and the Hamiltonian is the third term of the parent Hamiltonian for Gibbs distribution of 1-D Ising model.

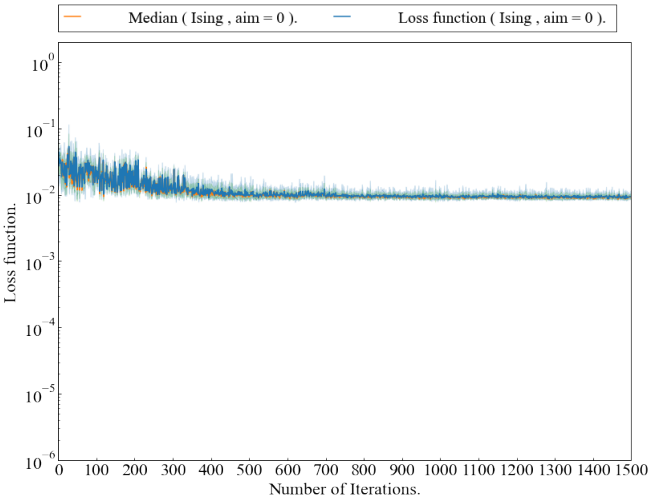

Fig. 8. The number of trials v.s. the average of the loss function for the quarter Grover's operator in case the initial state is the evenly distributed state, and the Hamiltonian is the All-to-All connected Ising model. The blue area is the realm of the distribution of loss function for 10 sampled values and the green hatched area is the standard deviation, respectively.

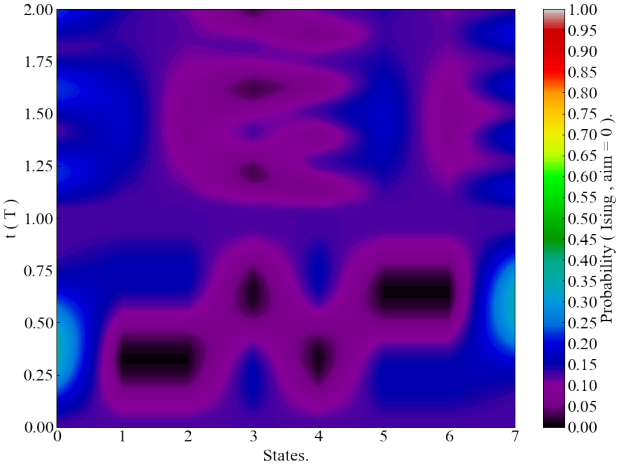

Fig. 9. The probability of states for a time expressed by gradation map at the best trial for the quarter Grover's operator in case the initial state is the evenly distributed state and the Hamiltonian is the All-to-All connected Ising model.

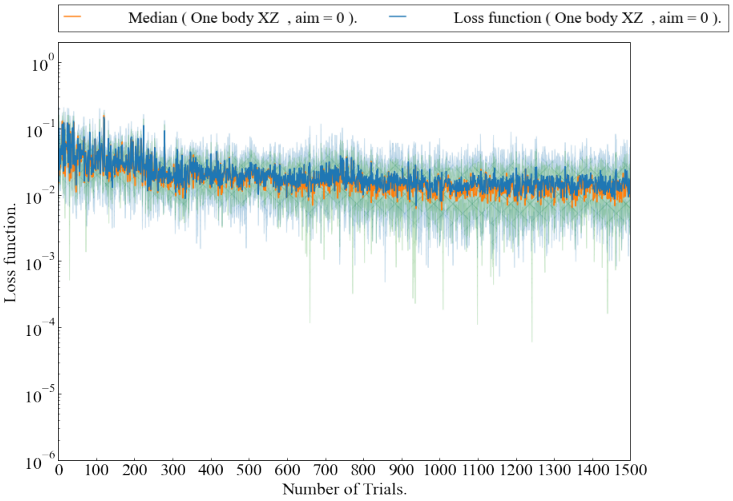

Fig. 10. The number of trials v.s. the average of the loss function for the quarter Grover's operator in case the initial state is the evenly distributed state and the Hamiltonian is the One-body Pauli X and Z model. The blue area is the realm of the distribution of loss function for 10 sampled values, and the green hatched area is the standard deviation, respectively.

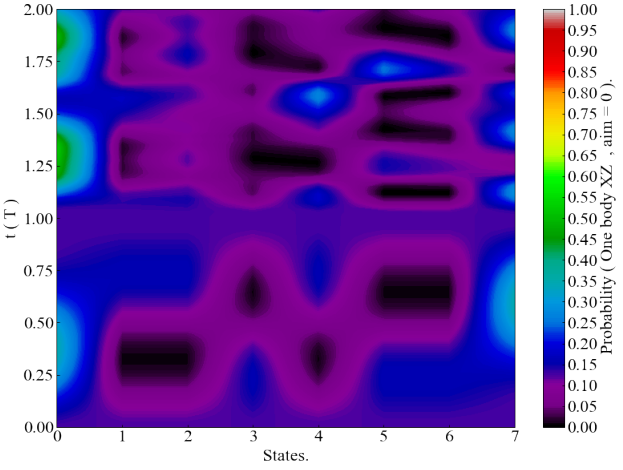

Fig. 11. The probability of states for time expressed by gradation map at the best trial for the quarter Grover's operator in case the initial state is the evenly distributed state and the Hamiltonian is the One-body Pauli X and Z model.

On the other hand, we optimized the parameters for the oracle operator aimed at the $|\ 0\rangle$ state. The Hamiltonian is one body X and Z operator with an oracle operator. The number of trials is 1500. We show the logarithmic loss function for the number of trials in Fig. 12. The loss function average is the minimum at the 917th trial, and the value is 66.4792. The minimum, maximum, and median of the 10 calculations are 66.1284, 66.8675, and 66.5017, respectively. We also show the propagation of the phases of states in Fig . 13, for the parameters on the trial. The phases of all states are off-aimed values. The number of qubits is 3, and ancilla is 1 qubit. We use eq. 3 for loss function and its $\boldsymbol{f}$ and $\boldsymbol{f^{aim}}$ are the coefficients derived by quantum tomography for this calculation. The number of valuable items includes the broadness of the noise. The realm of the parameter is [-4, 4) for all value components; universal quantum computation using QTCC is supposed to be limited.

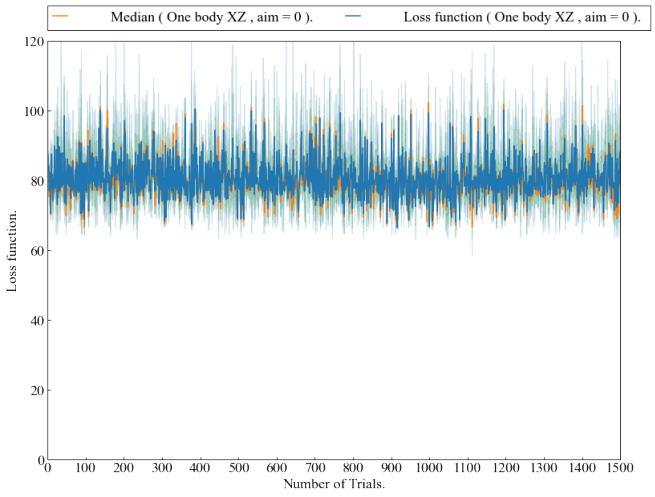

Fig. 12. The number of trials v.s. the average of the loss function for the oracle operator in case the initial state is the evenly distributed state, and the Hamiltonian is the One-body Pauli X and Z model. The blue area is the realm of the distribution of loss function for 10 sampled values, and the green hatched area is the standard deviation, respectively.

On the third hand, we optimize the parameters for Adiabatic Grover's algorithm [28]. The number of qubits is 3, and the noise Hamiltonian is,

$$H_1 = (1 - s/T)H_i + s/TH_f \tag{5}$$
$$H_i = \theta_0 I - \theta_1 \mid \psi\rangle\langle\psi \mid \tag{6}$$
$$H_f = \theta_0 I - \theta_2 \mid \psi\rangle\langle\psi \mid + \theta_3(\mid i\rangle\langle\psi \mid + \mid \psi\rangle\langle i \mid) \tag{7}$$

for the time s and the period T and the initial state $\mid \psi\rangle = \sum_{j=0} 1/\sqrt{2^n - 1} \mid j\rangle$ where $\mid \psi\rangle = \sum_{j=0} 1/\sqrt{2^n - 1} \mid j\rangle$ is the superposition of all states and $\mid i\rangle$ is an equal superposition of all states except for the aimed state. The number of trials is 300. Then, s starts from 0 at t = T and s = t-T after that. We calculate the loss function at t = 2T. As shown in Fig. 14, the average of the loss function lowers the fastest in above all cases, and the average reaches the minimum 8.2349 $\times 10^{-5}$ at the 189th trial. The minimum, maximum, and median are 1.7901 $\times 10^{-5}$, 1.799 $\times 10^{-4}$, and 1.806 $\times 10^{-5}$, respectively. Besides, the difference between maximum, minimum, and standard deviation is the smallest in all cases and trials. We show the time propagation for the parameter of all states in Figs. 15 and

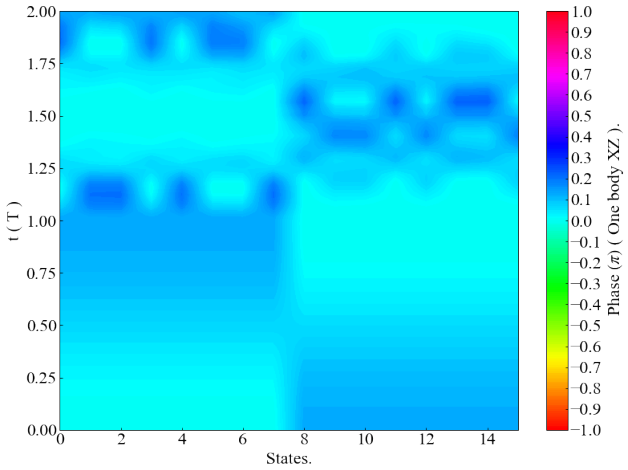

Fig. 13. The phase of states for time expressed by gradation map at the best trial for the oracle operator in case the initial state is the evenly distributed state and the Hamiltonian is the One-body Pauli X and Z model.

16. As shown in Fig. 15, the probability of $|0\rangle$ state lowers from t = T until t = 1.6T and becomes 1 by 2T. The phase of $|0\rangle$ state becomes π at T and stays after that, as shown in Fig. 16. The Hamiltonian is assembled compared to other cases, the QTCC has the potential for adiabatic quantum computation.

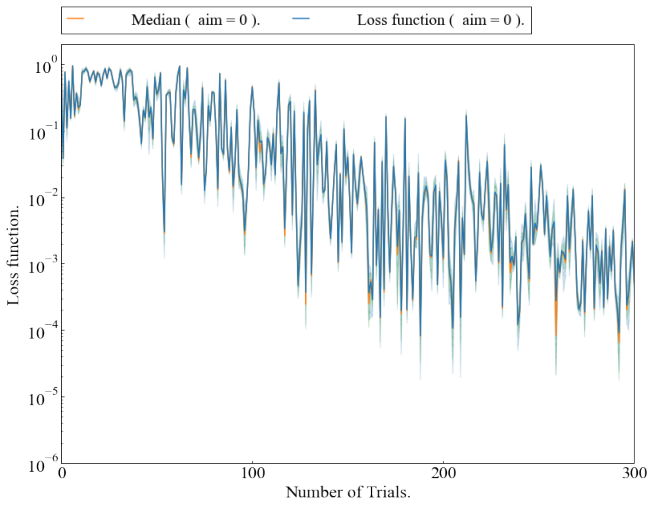

Fig. 14. The number of trials v.s. the average of the loss function for Adiabatic Grover's algorithm in case the initial state is the evenly distributed state, and the Hamiltonian is the eq. 7. The blue area is the realm of the distribution of loss function for 10 sampled values, and the green hatched area is the standard deviation, respectively.

4.2 Quantum Fourier Transformation

In this subsection, we describe the result of performing QFT using QTCC. For this calculation, we abide by the manner of subspace-search calculation, such as subspace-search VQE. We calculate multiple and $\boldsymbol{f}$ from multiple initial states and common ansatz. The entire loss function yields.

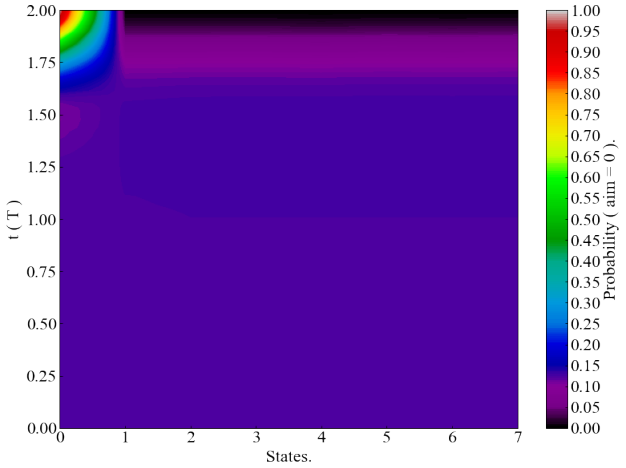

Fig. 15. The probability of states for time expressed by gradation map at the best trial for Adiabatic Grover's algorithm in case the initial state is the evenly distributed state, and the Hamiltonian is the 7.

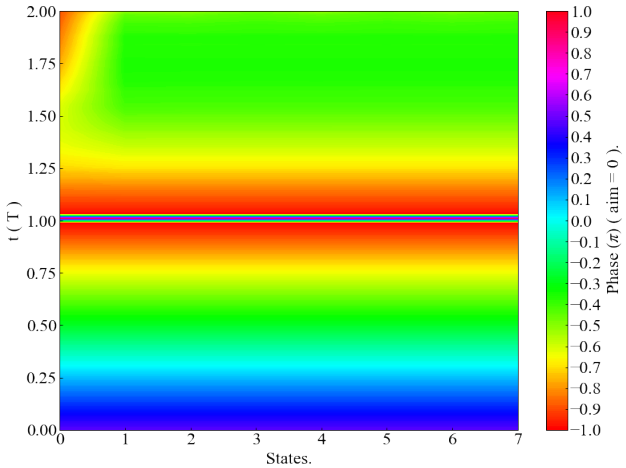

Fig. 16. The phase of states for time expressed by gradation map at the best trial for Adiabatic Grover's algorithm in case the initial state is the evenly distributed state, and the Hamiltonian is the 7.

The realm of the parameter is [-4, 4) for all value components from here.

$$F = \sum_{j=0} 1/(j+1)F_j \tag{8}$$

$$F_j = \boldsymbol{f_j} K \boldsymbol{f_j} + \boldsymbol{f_j^{aim}} K \boldsymbol{f_j^{aim}} - 2\boldsymbol{f_j^{aim}} K \boldsymbol{f_j}. \tag{9}$$

We assume that the initial states have three patterns of impulse and no probability periodicity. The initial states' periods are 16, 8, and 4, and the aimed states are spectrums from 0 by 16, 8, and 4, respectively. We show the logarithmic loss function for the number of trials in three initial states in Figs. 17, 18, and 19, respectively. For the initial state with period 16, the average loss function is minimum in the 283rd trial, and the values for the case where the periods of the initial states are 16, 8, and 4 are 4.799 $\times 10^{-2}$, 5.062 $\times 10^{-2}$ and 8.639 $\times 10^{-2}$, respectively.

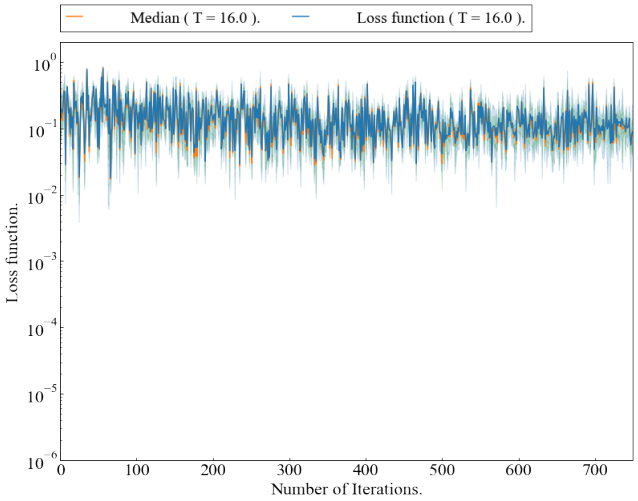

Fig. 17. The number of trials v.s. the average of the loss function for the spectrum from 0 by 16 in case the period of the initial state is 16, and the Hamiltonian is the One-body Pauli X and Z model. The blue area is the realm of the distribution of loss function for 10 sampled values and the green hatched area is the standard deviation, respectively.

QFT is also difficult for QTCC.

4.3 Adiabatic Shor's algorithm

In this section, we derive the parametric Hamiltonian for the Adiabatic Shor's algorithm [26] for factorization for 21. According to the paper, factorization of 21 can be performed by 3 qubits adiabatically. g is the coefficient for optimization derivation and is 30. The number of qubits is 3, and the Hamiltonian is,

$$H_1 = (1 - (s/T)^2)H_i + (s/T)^2 H_f \tag{10}$$

$$H_i = \theta_0 \sum_{j=0}^{N} X_j \tag{11}$$

$$\begin{aligned} H_f = \theta_1 (&210I + 84Z_0 + 88Z_1 + 44Z_2 - 20Z_0Z_1 - 10Z_0Z_2 \\ &+20Z_1Z_2 - 16Z_0Z_1Z_2) \end{aligned} \tag{12}$$

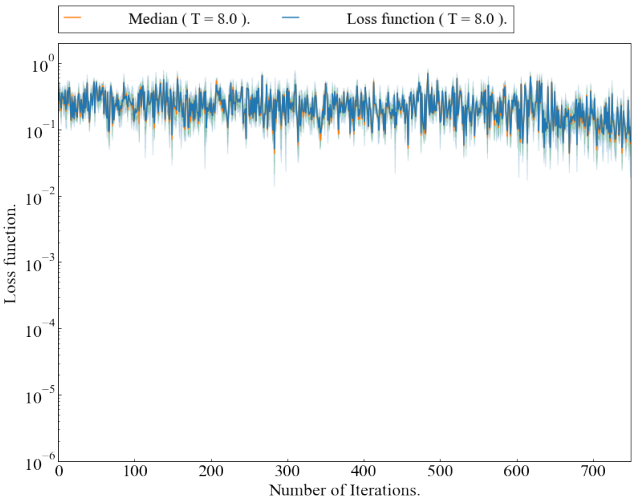

Fig. 18. The number of trials v.s. the average of the loss function for the spectrum from 0 by 8 in case the period of the initial state is 8, and the Hamiltonian is the One-body Pauli X and Z model. The blue area is the realm of the distribution of loss function for 10 sampled values, and the green hatched area is the standard deviation, respectively.

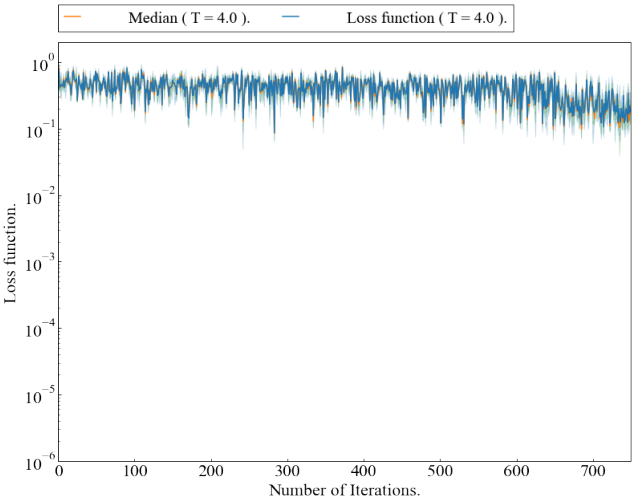

Fig. 19. The number of trials v.s. the average loss function for the spectrum from 0 by 4 in case the initial state is 4, and the Hamiltonian is the One-body Pauli X and Z model. The blue area is the realm of the distribution of loss function for 10 sampled values, and the green hatched area is the standard deviation, respectively.

for the time s and the period T And the initial state $\mid \psi\rangle = \prod_{j=0}^{N} H_j X_j \mid 0\rangle$.

The number of trials is 300. Then, s starts from 0 at t = T and s = t-T after that. We calculate the loss function at t = 2T. As shown in Fig. 20, the average of the loss function lowers the fastest in above all cases, and the average reaches the minimum 2.4569×10^{-5} at the 226th trial. The minimum, maximum and median are 6.4716×10^{-6}, 5.9159×10^{-5}, and 1.8173×10^{-5}, respectively. We also show the time propagation of the state for a case in Fig. 21. The states $\mid 3\rangle$ and $\mid 7\rangle$ increase from t = T to t = 1.5T. After that, the $\mid 3\rangle$ state is suppressed, and the $\mid 7\rangle$ state is amplified to 1 with respect to the probability. The number of parameters is only 2. However, the ability of QTCC to perform Adiabatic quantum computation is demonstrated enough.

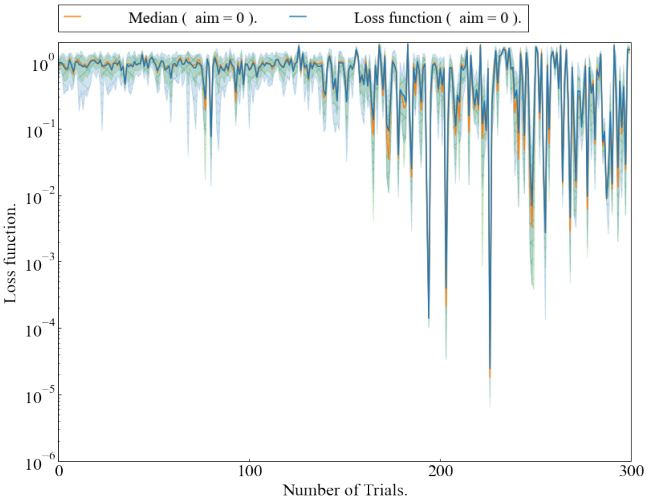

Fig. 20. The number of trials v.s. the average of the loss function for Adiabatic Shor's algorithm in case the initial state is $\mid \psi\rangle = \prod_{j=0}^{N} H_j X_j \mid 0\rangle$ and the Hamiltonian is the eq. 12. The blue area is the realm of the distribution of loss function for 10 sampled values and the green hatched area is the standard deviation, respectively.

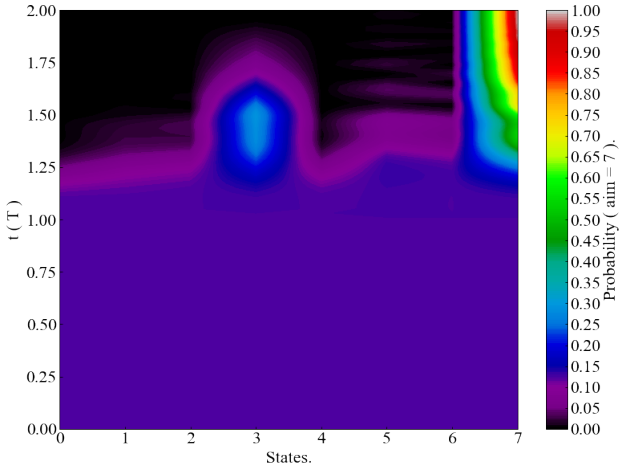

Fig. 21. The probability of states for time expressed by gradation map at the best trial for Adiabatic Shor's algorithm in case the initial state is $\mid \psi\rangle = \prod_{j=0}^{N} H_j X_j \mid 0\rangle$ and the Hamiltonian is the eq. 12.

5 discussion

QTCC demonstrates sensitivity to initial states similar to chaotic systems. At first, we confirm behavior by deriving the parameters that propagate the given single state and evenly distributed state to the given single states. We show the logarithmic minimum averages of loss functions for the aimed single state from the $|\,0\rangle$ state and from the evenly distributed state in Fig. 22, respectively. Fig. 22 shows that any single state from $|\,0\rangle$ to $|\,7\rangle$ can be reached accurately. In contrast, no single state can be reached by $t = 2T$.

The realm of the parameter is [0,2) for all value components here.

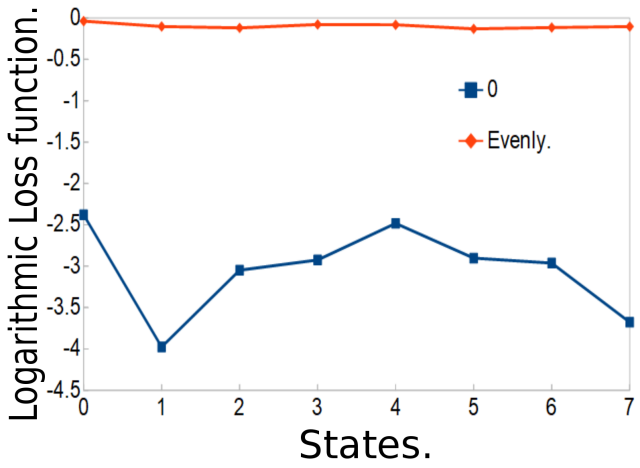

Fig. 22. The number of aimed state v.s. logarithmic loss function in case initial is $|\,0\rangle$ state and the evenly distributed state, respectively.

From these and the results in Section 3, the time propagation of QTCC retrieval has a degree of stability, and the potential of changing the state of $|\,0\rangle$ state is more significant than that of the evenly distributed state. This evenly distributed state is supposed to be the most stable. QTCC can accurately perform adiabatic quantum algorithms. This is supposed to be because the parametric Hamiltonian is time-dependent. The states of QTCC cycle the definitive trajectory partially due to the noise. The evolution of Hamiltonians charges the trajectory. In addition, this phenomenon breaks the stability due to the initial state. It is supposed that the constant parametric Hamiltonian corresponds to the center-of-mass force and is perturbed by noise, and the time evolution of the Hamiltonian corresponds to the time evolution of the trajectory.

According to the paper [9], the propagated state of discrete TC varies by the hyperparameter ϵ of Hamiltonian. Hence, adiabatic control of the amplitude and distribution of noise can manipulate the result of the time propagation of TCs even on 4-qubit systems. This paper also show the same result on 57-qubit system[10]. The controlling of parameters changes the result of time propagation even on 4-qubit systems. The noise and parametric Hamiltonian itself evolve over time, and the more complex the operation, the more complicated operation such as universal QFT may be realized. However, the limit of the number of gates and its variation for a single parameter set and Hamiltonian is still an open problem. The correspondence between the noise and parameter set and operation is also.

6 Concluding remarks

The paper reveals that the QTCC can accurately perform adiabatic quantum computation and universal gate operation. This means that more kinds of systems can perform adiabatic quantum computing and quantum computing. For example, hot and wet systems such as organic compounds and cells, especially neurons [34]. However, some objectives remain. The major objectives are establishing the method to calculate the parameters and perform adiabatic quantum computation accurately in case three or more noise parameters split the Hamiltonian complex and the method to perform universal quantum computation accurately.

Machine learning by the manner of recurrent neural network and quantum reservoir computing [11], and Variational Quantum Kolmogorov-Arnold Network (VQKAN) [37] is also. Regardless, quantum annealers and quantum computers can take advantage of the noise. Hence, the QTCC may be a milestone in quantum computing.

References

[1] Abanin, D.A., Altman, E., Bloch, I., Serbyn, M.: Colloquium: Many-body localization, thermalization, and entanglement. Reviews of Modern Physics **91**(2), 021001 (Apr 2019). https://doi.org/10.1103/RevModPhys.91.021001

[2] Abel, S., Criado, J.C., Spannowsky, M.: Completely quantum neural networks. Phys. Rev. A **106**(2), 022601 (Aug 2022). https://doi.org/10.1103/PhysRevA.106.022601

[3] Akiba, T., Sano, S., Yanase, T., Ohta, T., Koyama, M.: Optuna: A next-generation hyperparameter optimization framework. In: The 25th ACM SIGKDD International Conference on Knowledge Discovery & Data Mining. pp. 2623–2631 (2019)

[4] Autti, S., Heikkinen, P.J., Nissinen, J., Mäkinen, J.T., Volovik, G.E., Zavyalov, V.V., Eltsov, V.B.: Nonlinear two-level dynamics of quantum time crystals. Nature Communications **13**(1), 3090 (Jun 2022). https://doi.org/10.1038/s41467-022-30783-w, `https://doi.org/10.1038/s41467-022-30783-w`

[5] Chen, B., Li, S., Hou, X., Zhou, F., Qian, P., Mei, F., Jia, S., Xu, N., Shen, H.: Digital Quantum Simulation of Floquet Topological Phases with a Solid-State Quantum Simulator. arXiv e-prints arXiv:2012.05495 (Dec 2020). https://doi.org/10.48550/arXiv.2012.05495

[6] Cossins, M.J., Phang, S.: New Reservoir Computing Kernel Based on Chaotic Chua Circuit and Investigating Application to Post-Quantum Cryptography. arXiv e-prints arXiv:2406.12948 (Jun 2024). https://doi.org/10.48550/arXiv.2406.12948

[7] Cramer, M., Plenio, M.B., Flammia, S.T., Somma, R., Gross, D., Bartlett, S.D., Landon-Cardinal, O., Poulin, D., Liu, Y.K.: Efficient quantum state tomography. Nature Communications **1**(9), 149 (Dec 2010). https://doi.org/10.1038/ncomms1147

[8] Else, D.V., Monroe, C., Nayak, C., Yao, N.Y.: Discrete Time Crystals. Annual Review of Condensed Matter Physics **11**, 467–499 (Mar 2020). https://doi.org/10.1146/annurev-conmatphys-031119-050658

[9] Estarellas, M.P., Osada, T., Bastidas, V.M., Renoust, B., Sanaka, K., Munro, W.J., Nemoto, K.: Simulating complex quantum networks with time crystals. Science Advances **6**(42), eaay8892 (2020). https://doi.org/10.1126/sciadv.aay8892, `https://www.science.org/doi/abs/10.1126/sciadv.aay8892`

[10] Frey, P., Rachel, S.: Realization of a discrete time crystal on 57 qubits of a quantum computer. Science Advances **8**(9), eabm7652 (2022). https://doi.org/10.1126/sciadv.abm7652, `https://www.science.org/doi/abs/10.1126/sciadv.abm7652`

[11] Fujii, K., Nakajima, K.: Quantum reservoir computing: a reservoir approach toward quantum machine learning on near-term quantum devices. arXiv e-prints arXiv:2011.04890 (Nov 2020). https://doi.org/10.48550/arXiv.2011.04890

[12] Hansen, N.: The CMA Evolution Strategy: A Tutorial. arXiv e-prints arXiv:1604.00772 (Apr 2016). https://doi.org/10.48550/arXiv.1604.00772

[13] Havlíček, V., Córcoles, A.D., Temme, K., Harrow, A.W., Kandala, A., Chow, J.M., Gambetta, J.M.: Supervised learning with quantum-enhanced feature spaces. Nature **567**(7747), 209–212 (Mar 2019). https://doi.org/10.1038/s41586-019-0980-2

[14] Itoh, K., Masaki, Y., Matsueda, H.: Quantum Energy Teleportation and Entropy Change due to Feedback Control in One-Dimensional Heisenberg Model. arXiv e-prints arXiv:2305.03967 (May 2023). https://doi.org/10.48550/arXiv.2305.03967

[15] Jiang, Y.Z., Chen, Y.Y., Guan, X.W.: Understanding many-body physics in one dimension from the Lieb-Liniger model. Chinese Physics B **24**(5), 050311 (May 2015). https://doi.org/10.1088/1674-1056/24/5/050311

[16] Kato, T.: https://github.com/qaqarot. Opensource software development kit (2018), `https://blueqat.com/`

[17] Khoshaman, A., Vinci, W., Denis, B., Andriyash, E., Sadeghi, H., Amin, M.H.: Quantum variational autoencoder. Quantum Science and Technology **4**(1), 014001 (Jan 2019). https://doi.org/10.1088/2058-9565/aada1f

[18] Kieler, M.F.I.: Eigenstate entanglement in chaotic bipartite systems. Ph.D. thesis, Technical University of Dresden, Germany (May 2024)

[19] Kobayashi, K., Fujii, K., Yamamoto, N.: Feedback-driven quantum reservoir computing for time-series analysis. arXiv e-prints arXiv:2406.15783 (Jun 2024). https://doi.org/10.48550/arXiv.2406.15783

[20] Kwak, Y., Yun, W.J., Pyoung Kim, J., Cho, H., Choi, M., Jung, S., Kim, J.: Quantum Distributed Deep Learning Architectures: Models, Discussions, and Applications. arXiv e-prints arXiv:2202.11200 (Feb 2022)

[21] Liu, J.G., Wang, L.: Differentiable Learning of Quantum Circuit Born Machine. arXiv e-prints arXiv:1804.04168 (Apr 2018)

[22] Magán, J.M.: Black holes, complexity and quantum chaos. Journal of High Energy Physics **2018**(9), 43 (Sep 2018). https://doi.org/10.1007/JHEP09(2018)043

[23] Mori, T., Ikeda, T.N., Kaminishi, E., Ueda, M.: Thermalization and prethermalization in isolated quantum systems: a theoretical overview. Journal of Physics B Atomic Molecular Physics **51**(11), 112001 (Jun 2018). https://doi.org/10.1088/1361-6455/aabcdf

[24] Paredes, B., Widera, A., Murg, V., Mandel, O., Fölling, S., Cirac, I., Shlyapnikov, G.V., Hänsch, T.W., Bloch, I.: Tonks-Girardeau gas of ultracold atoms in an optical lattice. Nature **429**(6989), 277–281 (May 2004). https://doi.org/10.1038/nature02530

[25] Patoary, A.M., Vikram, A., Shou, L., Galitski, V.: Chaotic roots of the modular multiplication dynamical system in Shor's algorithm. Physical Review Research **6**(3), L032046 (Aug 2024). https://doi.org/10.1103/PhysRevResearch.6.L032046

[26] Peng, X., Liao, Z., Xu, N., Qin, G., Zhou, X., Suter, D., Du, J.: Quantum Adiabatic Algorithm for Factorization and Its Experimental Implementation. Phys. Rev. Lett. **101**(22), 220405 (Nov 2008). https://doi.org/10.1103/PhysRevLett.101.220405

[27] Rebentrost, P., Mohseni, M., Lloyd, S.: Quantum Support Vector Machine for Big Data Classification. Phys. Rev. Lett. **113**(13), 130503 (Sep 2014). https://doi.org/10.1103/PhysRevLett.113.130503

[28] Roland, J., Cerf, N.J.: Quantum search by local adiabatic evolution. Phys. Rev. A **65**(4), 042308 (Apr 2002). https://doi.org/10.1103/PhysRevA.65.042308

[29] Romero, J., Babbush, R., McClean, J.R., Hempel, C., Love, P., Aspuru-Guzik, A.: Strategies for quantum computing molecular energies using the unitary coupled cluster ansatz. arXiv e-prints arXiv:1701.02691 (Jan 2017)

[30] Sacha, K., Zakrzewski, J.: Time crystals: a review. Reports on Progress in Physics **81**(1), 016401 (Jan 2018). https://doi.org/10.1088/1361-6633/aa8b38

[31] Singh, H., McCulloch, E., Gopalakrishnan, S., Vasseur, R.: Emergence of Navier-Stokes hydrodynamics in chaotic quantum circuits. arXiv e-prints arXiv:2405.13892 (May 2024). https://doi.org/10.48550/arXiv.2405.13892

[32] Teh, J.S., Alawida, M., Sii, Y.C.: Implementation and practical problems of chaos-based cryptography revisited. Journal of Information Security and Applications **50**, 102421 (2020). https://doi.org/https://doi.org/10.1016/j.jisa.2019.102421, `https://www.sciencedirect.com/science/article/pii/S2214212619306544`

[33] Tilly, J., Chen, H., Cao, S., Picozzi, D., Setia, K., Li, Y., Grant, E., Wossnig, L., Rungger, I., Booth, G.H., Tennyson, J.: The Variational Quantum Eigensolver: A review of methods and best practices. Physics Reports **986**, 1–128 (Nov 2022). https://doi.org/10.1016/j.physrep.2022.08.003

[34] Toida, H., Sakai, K., Teshima, T.F., Hori, M., Kakuyanagi, K., Mahboob, I., Ono, Y., Saito, S.: Magnetometry of neurons using a superconducting qubit. Communications Physics **6**(1), 19 (Feb 2023). https://doi.org/10.1038/s42005-023-01133-z, `https://doi.org/10.1038/s42005-023-01133-z`

[35] Vorobyov, V., Zaiser, S., Abt, N., Meinel, J., Dasari, D., Neumann, P., Wrachtrup, J.: Quantum Fourier transform for nanoscale quantum sensing. npj Quantum Information **7**, 124 (Jan 2021). https://doi.org/10.1038/s41534-021-00463-6

[36] Wakaura, H., Bayu Suksmono, A.: Derivation of Hamiltonians from time propagations using Born machines. arXiv e-prints arXiv:2312.16432 (Dec 2023). https://doi.org/10.48550/arXiv.2312.16432

[37] Wakaura, H., Bayu Suksmono, A., Mulyawan, R.: Variational quantum kolmogorov-arnold network. Research Square (2024). https://doi.org/10.21203/rs.3.rs-4504342/v3, https://doi.org/10.21203/rs.3.rs-4504342/v3, pREPRINT (Version 3)
[38] Wensink, H.H., Dunkel, J., Heidenreich, S., Drescher, K., Goldstein, R.E., Löwen, H., Yeomans, J.M.: Meso-scale turbulence in living fluids. Proceedings of the National Academy of Science **109**(36), 14308–14313 (Sep 2012). https://doi.org/10.1073/pnas.1202032109
[39] Wilczek, F.: Quantum Time Crystals. Phys. Rev. Lett. **109**(16), 160401 (Oct 2012). https://doi.org/10.1103/PhysRevLett.109.160401
[40] Zhang, B., Liu, L.: Chaos-based image encryption: Review, application, and challenges. Mathematics **11**(11) (2023). https://doi.org/10.3390/math11112585, https://www.mdpi.com/2227-7390/11/11/2585
[41] Zhong, D., Wu, Q., Zhang, J., Wang, T., Chen, Y., Zeng, H., Ren, Z., Wang, Y., Qiu, C.: Exploration of a brain-inspired photon reservoir computing network based on quantum-dot spin-VCSELs. Optics Express **32**(16), 28441 (Jul 2024). https://doi.org/10.1364/OE.527428

Authors

Hikaru Wakaura Gained PhD of technology at Tsukuba University in Japan in 2017, worked at blueqat as a quantum algorithm researcher from 2018 till 2019, worked at Quantinuum in 2022, and independent researcher for now. Main research areas are quantum hardware and quantum algorithm.

Andriyan B. Suksmono Professor of Imaging and Signal Processing in the School of Electrical Engineering and Informatics, ITB (Institut Teknologi Bandung), Indonesia. He received Sarjana (BSc.) in Physics and Magister (M.S.) in Electrical Engineering from ITB and a PhD degree from Faculty of Engineering, The University of Tokyo, Japan. His main research interests are Compressive Sampling, Radar, Subsurface Imaging, and Quantum Computing.

© 2025 By AIRCC Publishing Corporation . This article is published under the Creative Common Attribution (CC BY) license.